Plasma arc behaviour in direct current arc furnace smelting of platinum group metal-bearing materials: A modelling study on the effect of reductant choice

by Q.G. Reynolds[1,2], B.S. Xakalashe[1], S.P. Tsebe[1], M.W. Erwee[3], I.J. Geldenhuys[4], R.T. Jones[4]

Affiliation:
[1]Mintek, South Africa
[2]Stellenbosch University, South Africa
[3]Samancor Chrome Ltd, South Africa
[4]Independent Consultant, South Africa

Correspondence to:
Q.G. Reynolds

Email:
quinnr@mintek.co.za

Dates:
Received: 19 Oct. 2025
Published: February 2026

How to cite:
Reynolds, Q.G., Xakalashe, B.S., Tsebe, S.P., Erwee, M.W., Geldenhuys, I.J., Jones, R.T. 2026. Plasma arc behaviour in direct current arc furnace smelting of platinum group metal-bearing materials: A modelling study on the effect of reductant choice. *Journal of the Southern African Institute of Mining and Metallurgy*, vol. 126, no. 2, pp.125–134

DOI ID:
https://doi.org/10.17159/2411-9717/PGM30/2026

ORCiD:
Q.G. Reynolds
http://orcid.org/0000-0002-5196-8586

This paper is based on a presentation given at the 9TH International PGM Conference 2025, 27-28 October 2025, Sun City, Rustenburg, South Africa

Abstract

Aspects of the production of platinum group metals by reductive smelting in direct-current arc furnace processes are investigated using a computational modelling approach. The replacement of fossil carbon as a reductant by alternative reductants such as silicon carbide, ferrosilicon, and hydrogen is desirable for reducing direct greenhouse gas emissions from such processes, but the impact of these changes on the electrical operability of the process is poorly understood. This paper presents a study of plasma arc behaviour in the context of the ConRoast® reductive smelting process for Upper Group 2 ore as well as processes for recycling of automotive catalysts, using an integrated computational modelling workflow. It was found that the freeboard gas compositions, plasma properties, and arc behaviour were all affected by the choice of reductant, particularly in carbon-free smelting using ferrosilicon or hydrogen.

Keywords

PGMs, Pyrometallurgy, DC furnace, Modelling

Introduction

Platinum group metals (PGM) production by alloy smelting in open-bath direct current (DC) electric arc furnaces offers an alternative to traditional matte smelting processes, and may be used for both primary and secondary raw materials (Jones, 2015). Such processes use a chemical reductant to transform metal oxides in the furnace feed into an alloy collector phase, into which the PGM content is preferentially concentrated prior to further refining.

For smelting of primary sulphide concentrates with high chromite content, such as those obtained from the mining of Upper Group 2 (UG2) reserves in South Africa, the ConRoast® process is an attractive option (Jones, 2002; Phillips et al., 2008). This is a multi-step flowsheet starting with oxidative dead-roasting of concentrate fines in a fluidised bed reactor to convert sulphides to oxides and capture the sulphur oxide emissions for sulphuric acid production, followed by reductive smelting of the oxides in a DC arc furnace (see Figure 1). This produces an iron-rich alloy containing the base metals (nickel, cobalt, and copper) and the PGMs. The molten alloy is atomised to render it amenable to downstream hydrometallurgical methods for base metals and PGM refining.

Another growing application of alloy smelting is the recycling of spent catalytic converters (autocats) from the automotive industry (Benson et al., 2000; Peng et al., 2017). These typically contain small quantities of PGMs, which are coated on the surfaces of a porous ceramic substrate typically made of cordierite ($2MgO.2Al_2O_3.5SiO_2$). In some cases, particularly in autocats originating from the heavy-duty vehicle market, the substrate may also contain silicon carbide (SiC). The autocat material is fed to a DC arc furnace with an iron source such as hematite and a chemical reductant (only necessary if the autocat SiC content is insufficient to complete the reaction). This again produces an iron-rich alloy with the collected base metals (mainly nickel) and PGMs. The alloy generated in this process typically contains high levels of iron (85% – 90% Fe), which is not suitable for downstream refining. As such, the iron alloy is first oxygen refined in a converting process to remove most of the iron before sent to downstream refining for recovery of the base metals and PGMs. A typical flowsheet for processing of spent autocats is shown in Figure 2.

A challenge with many existing reductive smelting processes is their reliance on fossil carbon as a reductant, which can generate significant scope-1 greenhouse gas emissions. Although an increasing number of low-carbon alternative reductants such as silicon carbide (Malan et al., 2015), ferrosilicon alloys (Akhmetov et al., 2025), hydrogen (Dalaker, Hovig, 2023), and others, are currently available or

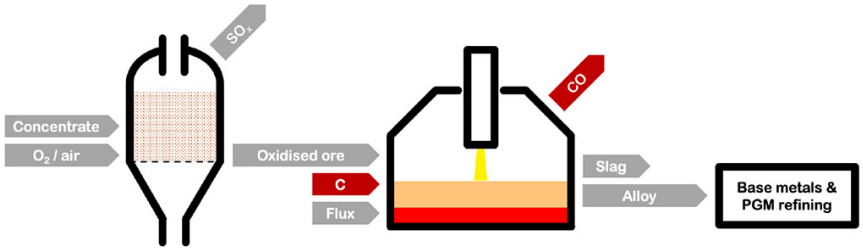

Figure 1—Simplified ConRoast® process flowsheet

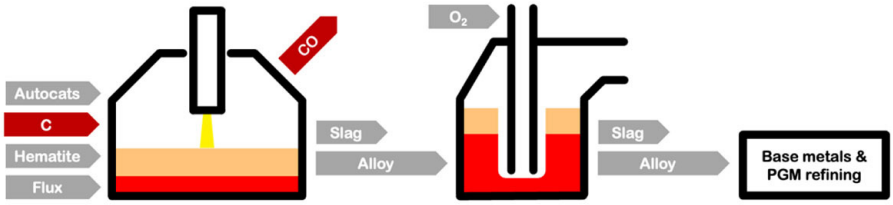

Figure 2—Simplified flowsheet for processing of spent autocats in DC furnace via the alloy-collector method

Figure 3—Integrated computational modelling workflow for plasma arc behaviour

becoming so, the replacement of fossil carbon with these materials in PGM alloy smelting is still largely untested and may result in undesirable operational conditions for the smelting furnace. In particular, the process chemistry of using carbon-free reductants such as ferrosilicon and hydrogen is likely to cause significant differences in the chemical composition of the gas phase inside the furnace vessel. This, in turn, may alter the electrical and dynamic behaviour of the plasma arc in applications where a DC arc furnace is used for the reductive smelting step.

The literature on modelling the influence of alternative reductants and process chemistry on plasma arc behaviour is rather sparse. Recent computational multiphysics studies on arcs in hydrogen have however shown that the effect can be substantial, with the high resistivity and low density of plasmas generated from hydrogen and hydrogen/water mixtures resulting in unstable arc operation (Al Nasser et al., 2024). Numerical calculation of plasma properties for different metallurgical processes has also demonstrated that even relatively small differences in minor contaminants in the gas phase can have a disproportionately large effect on properties such as electrical conductivity and thermal radiation, to which arc behaviour is sensitive (Reynolds et al., 2025a). It would therefore seem prudent to apply arc modelling workflows to study the effect of alternative reductant choices in PGM alloy smelting, so that potential difficulties in moving to low-carbon processes can be identified and mitigated well in advance of any real-world implementations.

Theory and model description

The plasma arc in a DC arc furnace is a very fast (km/s), very hot (> 10000 K) jet formed by electromagnetic forces acting on thermally ionised gases in the freeboard space above the molten bath of process material (Bowman, Krüger, 2009). Its ability to conduct electricity and transfer large amounts of mechanical and thermal energy to the bath makes it the *engine room* of the furnace. Understanding the behaviour of the arc and the region immediately around it correctly, is therefore key to the effective operation of DC arc furnace processes (Geldenhuys, 2017).

Due to the extreme conditions under which they operate, the large-scale arcs used in metallurgical processing are challenging to study experimentally. Computational models based on mathematical descriptions of the physics describing plasma arcs have however advanced rapidly in recent years, and offer a useful alternative for investigating arc behaviour in response to changes in process conditions. Modern approaches to modelling plasma arcs make use of integrated workflows including the effect of metallurgical chemistry on the plasma gas composition and the influence of the gas composition on the resulting plasma's thermophysical properties (Reynolds et al., 2025a). The modelling workflow used in the present study is shown in Figure 3.

The first step in the workflow uses tools such as FactSage (Bale et al., 2016) to perform thermodynamic equilibrium calculations for the metallurgical process in question. In the case of PGM, smelting calculations were performed using appropriate alloy and oxide databases for the slag and alloy phases, and ideal mixture data for the gas phase – further case-specific details are provided in the results section. Multiphase thermodynamic equilibria were obtained based on the feed material composition and process temperature in each case to yield the composition of species in the gas phase.

The gas compositions were passed into an open-source calculator for plasma properties, minplascalc (Reynolds et al., 2025a, 2025b). The equilibrium composition of molecules, atoms, ions, and electrons was first calculated for each case using Gibbs free energy minimisation based on quantum mechanics descriptions of the internal energy and partition functions for each species. The plasma compositions were then used to calculate thermodynamic (density, enthalpy, and heat capacity) and transport (viscosity, electrical conductivity, thermal conductivity, and radiation emission coefficient) properties of plasmas as a function of temperature at atmospheric pressure. The plasma property data was then tabulated in an efficient lookup-table format for further use.

The final step in the modelling workflow involves using a specialised open-source computational mechanics solver, plasmaArc (Reynolds, 2025), to calculate the spatial and temporal evolution of a simulated arc for each case. The solver is implemented using the OpenFOAM® open-source framework (OpenCFD Ltd, 2025). It calculates numerical solutions to the governing equations of magnetohydrodynamics (MHD) involving three pieces of physics: fluid flow, heat transfer, and electromagnetic fields. These are described by a set of coupled non-linear partial differential equations as shown in Equations 1, 2, and 3.

$$\begin{aligned} &\nabla \cdot \mathbf{j} = 0, \qquad \text{with } \mathbf{j} = -\sigma\left(\nabla\phi + \frac{\partial \mathbf{A}}{\partial t} - \mathbf{u}\times\mathbf{B}\right) \\ &\nabla^2\mathbf{A} = -\mu_0\mathbf{j}, \qquad \text{with } \mathbf{B} = \nabla\times\mathbf{A} \end{aligned} \quad [1]$$

$$\begin{aligned} &\frac{\partial}{\partial t}(\rho h) + \nabla\cdot(\rho\mathbf{u}h) = \nabla\cdot(\kappa\nabla T) + \nabla\cdot\left(\frac{5k_B T}{2e}\mathbf{j}\right) + \frac{\mathbf{j}\cdot\mathbf{j}}{\sigma} + Q_m - Q_R \\ &Q_m = \nabla\cdot(\boldsymbol{\tau}_{ij}\cdot\mathbf{u}) - \frac{\partial}{\partial t}(\rho K) - \nabla\cdot(\rho\mathbf{u}K) + \frac{\partial P}{\partial t} \end{aligned} \quad [2]$$

$$\begin{aligned} &\nabla \cdot \mathbf{j} = 0, \qquad \text{with } \mathbf{j} = -\sigma\left(\nabla\phi + \frac{\partial \mathbf{A}}{\partial t} - \mathbf{u}\times\mathbf{B}\right) \\ &\nabla^2\mathbf{A} = -\mu_0\mathbf{j}, \qquad \text{with } \mathbf{B} = \nabla\times\mathbf{A} \end{aligned} \quad [3]$$

In Equations 1, 2, and 3, ρ is the plasma density, $\mathbf{u}$ is the velocity field, P is the pressure, τ_{ij} is the viscous stress tensor, $\mathbf{j}$ is the current density, $\mathbf{B}$ is the magnetic field vector, h is the plasma enthalpy field, κ is the thermal conductivity, T is the temperature field, σ is the electrical conductivity, $K = {}^1/_2|\mathbf{u}|2$ is the kinetic energy of the fluid, Q_R is the thermal radiation loss term, ϕ is the electric potential, and $\mathbf{A}$ is the magnetic vector potential.

Furthermore, Equations 1,2, and 3 are solved numerically subject to standard boundary conditions described in previous work on plasma arc models (Reynolds, 2020) with the exception of the temperature field. For this study, a new temperature boundary condition was developed based on physics-aware descriptions of near-electrode plasma sheath layers, following the unified cathode/anode sub-model (CASM) approach (Sævarsdóttir et al., 2006). The heat flux from the plasma to the boundary is simplified as the sum of contributions from local conduction and convection, thermal radiation, and electric current transport:

$$q_B = -\kappa\left.\frac{\partial T}{\partial \mathbf{n}}\right|_B + q_r - W_f j_e + U_i j_i \quad [4]$$

In Equation 4, $\mathbf{n}$ is a unit vector normal to the boundary surface and facing out of the computational domain, q_r is the net radiation flux into the surface from the thermal radiation sub-model in the MHD solver, W_f is the work function of the boundary material, U_i is the effective first ionisation potential of the plasma (taken as the minimum ionisation potential of all neutral species present), j_e is the electron current density at the boundary, and j_i is the ion current density. In addition, j_e and j_i are estimated at each boundary element using expressions modified from Lowke et al. (1997):

$$j_i = \max(\mathbf{j_B}\cdot\mathbf{n} - j_R, 0) \quad [5]$$

$$j_e = \mathbf{j_B}\cdot\mathbf{n} + j_i \quad [6]$$

$$j_R = A_{RD}T_B^2\exp\left(-\frac{q_e W_f}{kT_B}\right) \quad [7]$$

In expressions 5, 6, and 7, $\mathbf{j_B}$ is the net current density vector field at the boundary, jR is the thermionic emission current density, A_{RD} is the Richardson-Dushman thermionic emission coefficient, q_e is the elementary charge, k is the Boltzmann constant, and T_B is the temperature field at the boundary.

Once the total heat flux q_B is calculated, it is then used in a simple lumped parameter energy balance on each surface element of the boundary mesh to obtain its temperature:

$$\rho_B C_{P,B}\delta_B\frac{dT_B}{dt} = q_B - h_B(T_B - T_\infty) \quad [8]$$

In Equation 8, δ_B is the thickness of the thermally active layer of boundary material, and h_B is the thermal resistance between the boundary surface and its interior, which is assumed to be at temperature T_∞. These are both empirical parameters, with Equation 8 approximating complex transient heat transfer effects within the electrode and molten bath boundaries. The maximum values of T_B calculated from Equation 8 were also clamped at the vaporisation temperature T_v of the boundary material, providing a crude approximation of phase change behaviour.

Results and discussion

To study the effect of using alternative reductants in PGM alloy smelting, a case matrix was identified using two raw materials, ConRoast® oxidised concentrate and recycled autocats, and four different reductants: metallurgical coke, silicon carbide (SiC), ferrosilicon (FeSi), and hydrogen (H_2). Phase compositions for each combination of raw material and reductant were obtained from thermochemical modelling at a range of different slag bath temperatures extending from a representative bulk process temperature, 1650°C, to the point at which the majority of the alloy reports to the gas phase, approximately 2500°C. Such elevated slag temperatures are possible in the attachment zone where the arc connects to the slag bath surface (Barcza et al., 1990). The gas compositions for each combination of raw material, reductant, and slag temperature were then used to calculate the associated plasma properties as a function of plasma temperature, and the properties were passed into the MHD arc solver. For each set of process conditions, two model furnaces were simulated – one at 5 kA current scale representing a large pilot plant or small recycling facility, and one at 50 kA representing an industrial smelter. Transient arc voltages were extracted from the simulations and analysed further to identify trends and potential problems.

Thermochemical simulations

For each combination of raw material, reductant, and slag temperature, FactSage 8.3 was used to calculate the equilibrium phase compositions. The thermodynamic modeling employed multiple databases to ensure accurate representation of the different phases present in the system. For the slag and other oxide phases, solutions from the FTOxid database were used, while the SGTE database was employed for the alloy phase. Pure compound and gas data were sourced from the FactPS database, which included solid CeO_2 for the autocats simulations. Where viscosity calculations were required, the integrated viscosity model in FactSage was applied. Equilibrium calculations were performed using the "Equilib" module with a temperature step size of 5 K. Normal equilibrium mode was selected when solid reductants (coke, FeSi, SiC) were employed. For reduction involving H_2/Ar mixtures, the open option was used. In this configuration, equilibrium calculations are performed stepwise with small amounts of fresh reducing gas introduced to the system at each step, while the off-gas is discarded before the subsequent step. This approach effectively simulates continuous reducing gas flow into the reactor. The assumed compositions for the roasted concentrate from the ConRoast® process (Jones, 2002) and the feedstock for the autocats (Morcali, 2020) are shown in Table 1.

Table 1

Feed material compositions assumed

Raw material	Al_2O_3	C	CaO	Co	Cr_2O_3	FeO	MgO	Ni	S	SiO_2	CeO_2	ZrO_2
Roasted concentrate excl. Cu (ConRoast®)	5.4	0.09	4.3	0.06	2.7	16.3	19.9	1.84	0.25	43.3	-	-
Autocats excl. SiC	45.43	-	-	-	-	-	9.3	-	-	38.26	4.12	2.9

The platinum group metals (PGM) in the ConRoast® feed were assumed to be present as Pt (296 g/t), while values for Pt, Pd, and Rh were taken as 25, 54, and 8.5 g/t, respectively.

Several assumptions were made regarding the composition and properties of the reductants used in the simulations. Coke was assumed to have a dry fixed carbon content of 95%, with 5% volatiles and 0.5% moisture content, and no ash present. The volatiles were represented as CH_4 in the simulations for thermodynamic consistency. FeSi was assumed to consist of 75% Si and 25% Fe, while SiC was considered to be pure. All gases, including H_2 and inert gases (N_2 and Ar), were assumed to be pure. The reducing gas mixture for H_2/Ar reduction consisted of 30% H_2 and 70% Ar by volume. For cases involving FeSi reduction, sufficient N_2 was added to maintain a partial pressure of nitrogen (pN_2) of 0.98 atm at the bulk process temperature.

ConRoast® process simulations

For the ConRoast® process simulations, specific conditions were established for reductant addition and fluxing operations. The amount of coke added was set at 5 mass% of the total feed, based on the recipe described in Jones (2002). The quantity of FeSi added was calculated stoichiometrically to achieve full reduction of FeO and Cr_2O_3. To counteract the formation of SiO_2 as a reduction product, pure MgO was added to maintain an MgO/SiO_2 ratio of 0.48 at the bulk process temperature. This ratio was selected based on the composition reported for slag produced in the ConRoast® process (Jones, 2002). The same methodology was applied for SiC reduction cases. For reduction using H_2, eighteen steps of gas addition to the system were required to achieve a residual FeO content of 5% in the slag. This target was selected to match the level quoted in the ConRoast® process literature (Jones, 2002), ensuring comparable reduction levels between hydrogen and coke reduction scenarios.

The gas phase composition results from the equilibrium calculations are given in Figure 4. Only the total elemental composition is shown for easier comparison between cases. As a mined and processed ore, the ConRoast® raw material is metallurgically complex, and as a result the associated gas compositions are rich in trace metals such as copper, magnesium, nickel, and others. Sulphur is also a significant component in the ConRoast® gas compositions at higher temperatures. These are present in addition to the major species (carbon monoxide in the case of coke and SiC smelting, nitrogen in the case of FeSi, and unreacted hydrogen in the case of H_2). In all cases it can be seen that the trace elements become increasingly volatile as slag temperatures rise.

Autocat process simulations

The autocat smelting process requires the addition of hematite (assumed to be pure Fe_2O_3), which is reduced to form an iron alloy that serves as a collector for precious metals. The quantities

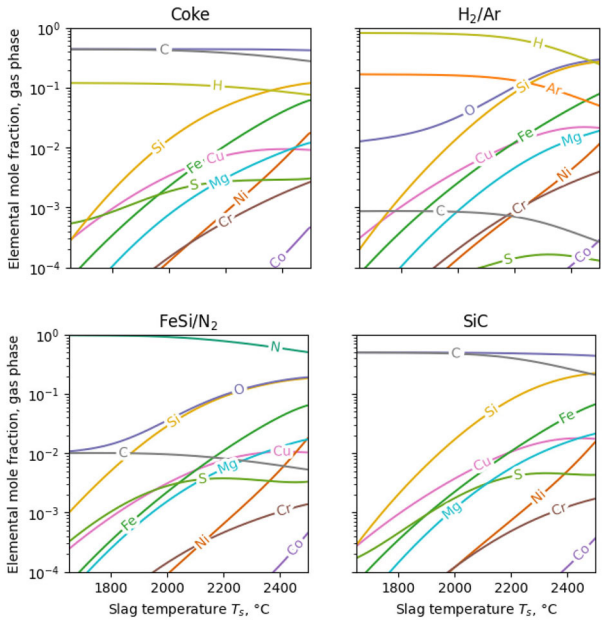

Figure 4—Equilibrium gas compositions in ConRoast® oxidised concentrate smelting

of hematite and flux added were based on industrial process data reported in Benson et al. (2000). For every 100 grams of autocat material, 114.3 grams of hematite was required. Fluxing was accomplished using CaO in all cases, with additions of 6 to 7 grams per 100 grams of autocat material. This fluxing strategy was designed to ensure a slag viscosity of less than 3 Pa.s at the bulk process temperature. The amounts of coke, FeSi, and SiC were calculated stoichiometrically to achieve complete reduction of the added hematite. For hydrogen reduction, the same stepwise approach used in the ConRoast® case was employed. In cases involving FeSi reduction, an inert nitrogen atmosphere was maintained following the same protocol established for the ConRoast® process.

The equilibrium gas phase composition results for autocat processes are given in Figure 5. Autocat raw materials are much simpler than the complex natural ores used in ConRoast®, and this results in a correspondingly simpler gas phase composition. The elements present in any significant quantities are however very similar, especially at low temperatures where the slag species are less volatile.

The absence of any PGM elements in the gas phase of both processes may seem somewhat contradictory at first, however, it should be recalled that although they are the primary product they are present in only very small quantities (ppm) in the raw materials. In addition, PGMs are not particularly volatile in elemental form at the slag temperatures considered here.

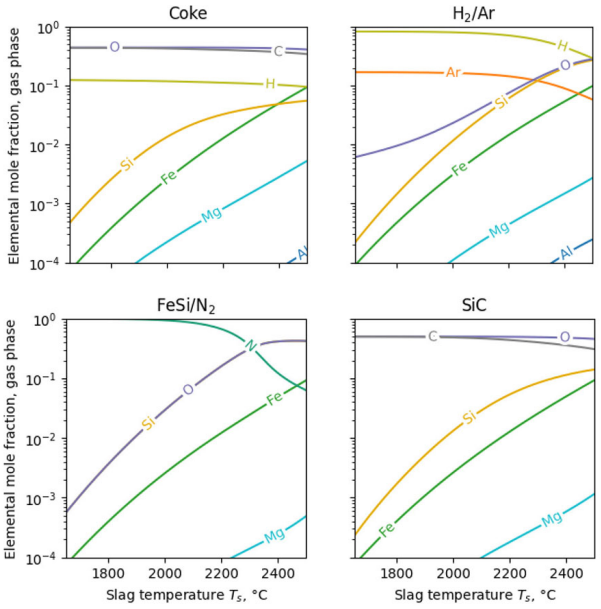

Figure 5—Equilibrium gas compositions in autocat smelting

Plasma property calculations

The elemental gas compositions for each combination of raw material, reductant, and slag temperature were passed into a parallelised scripted calculation of the associated thermophysical properties of the plasma. The full set of plasma species included Al, Ar, C, Co, Cr, Cu, Fe, H, Mg, N, Ni, O, S, Si, Al^{z+}, Ar^{z+}, C^{z+}, Co^{z+}, Cr^{z+}, Cu^{z+}, Fe^{z+}, H^{+}, Mg^{z+}, N^{z+}, Ni^{z+}, O^{z+}, S^{z+}, Si^{z+}, CO, CO_2, CrO, FeO, H_2, H_2O, H_2S, MgO, N_2, NO, NiO, OH, SO, SO_2, SiO, and SiS (where z is the ion charge number ranging between 1 and 3). These calculations were performed with minplascalc 1.0.2, and the necessary quantum mechanical data for each species were obtained from a variety of sources as documented elsewhere (Reynolds et al., 2025a). To improve calculation performance, species were omitted in cases where their constituent elements were not present in any significant amount in the original gas composition obtained from FactSage. The plasma composition and property calculations were then run between 300 K and 30000 K at a pressure of one atmosphere. At temperatures below 2000 K it was necessary to use reduced species sets to avoid numerical difficulties arising from charged particle concentrations dropping below machine precision. The full set of results, including gas compositions and plasma properties, is available online as an open dataset (https://zenodo.org/records/17063718, https://doi.org/10.5281/zenodo.17063718).

Plasma properties for process cases using metallurgical coke as a reductant are shown in Figure 6. In addition to the high degree of nonlinearity typical of plasma properties in general, it can be seen that there is almost no difference between the ConRoast® and autocat processes at lower slag temperatures. At high slag temperatures, the trace elements present begin to affect the properties more strongly, but even at T_s = 2500°C there are only relatively small differences between the two raw materials.

Properties for cases using SiC as a reductant are shown in Figure 7. A comparison with Figure 6 shows that there is a great deal of similarity in the plasma properties between processes using coke and SiC as a reductant, because the equilibrium gas phase in both cases is dominated by carbon and oxygen. Even though substantially less total carbon is expected to be emitted when using SiC, there would be relatively little difference in the gas environment in the freeboard of the furnace.

Moving on to FeSi as a reductant, the results are shown in Figure 8. Due to the large change in the equilibrium gas compositions for FeSi processes in which N_2 is used as a purge and dominates the gas atmosphere, the properties are quite different

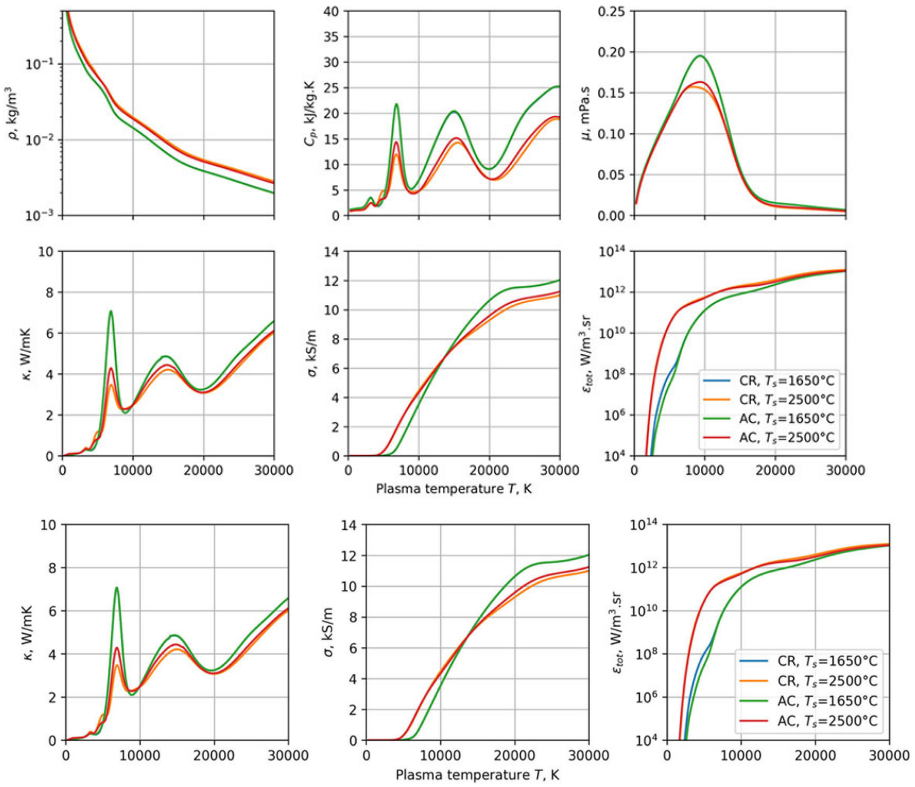

Figure 6—Plasma properties for cases using metallurgical coke as a reductant (CR = ConRoast®, AC = autocats)

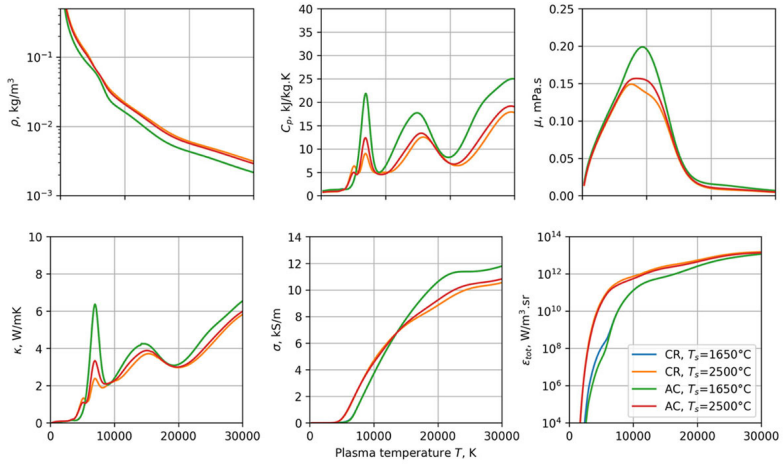

Figure 7—Plasma properties for cases using SiC as a reductant (CR = ConRoast®, AC = autocats)

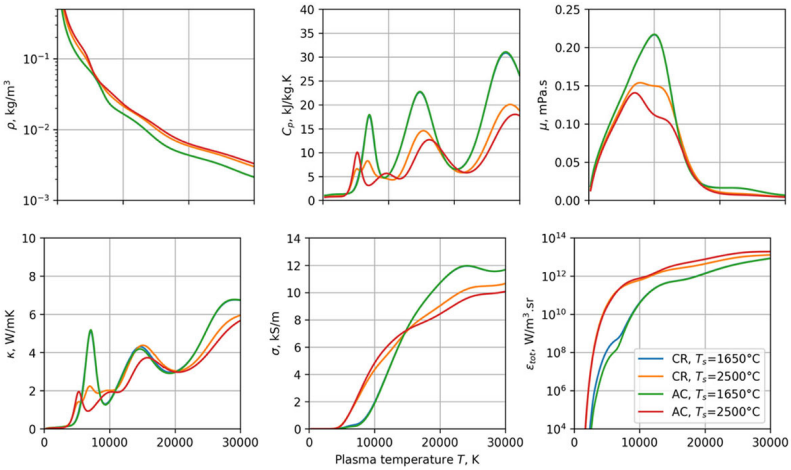

Figure 8—Plasma properties for cases using FeSi as a reductant (CR = ConRoast®, AC = autocats)

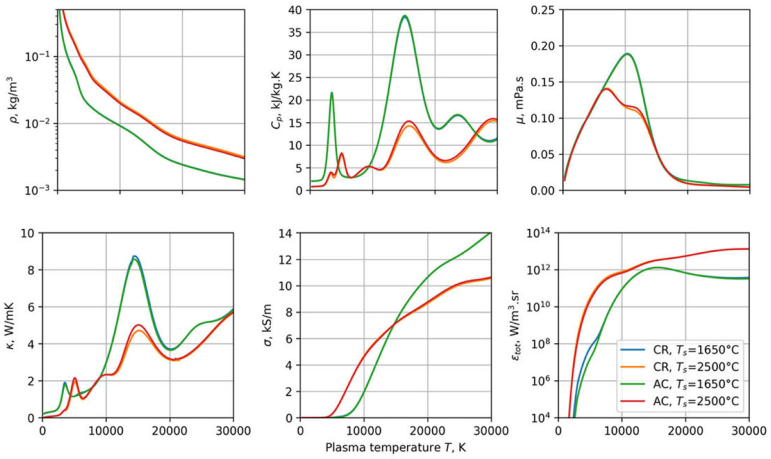

Figure 9—Plasma properties for cases using H_2 as a reductant (CR = ConRoast®, AC = autocats)

to those of coke and SiC processes. In particular, at lower slag temperatures the plasma is less electrically conductive and emits more thermal radiation in the important 5000 K – 15000 K range in which the main column of a plasma arc generally operates. This can be expected to affect the thermal and electrical behaviour of the arc appreciably.

Finally, process cases using H_2 as a reductant are compared in Figure 9. Because of the very low density and unusual quantum mechanical properties of hydrogen, this results in large differences in the properties of the plasma that would be generated by the freeboard gas, particularly at lower slag temperatures. The presence of argon as a carrier gas helps to ameliorate this to some degree, but the plasma density is low, and the heat capacity and thermal conductivity are very high. The electrical conductivity and emission coefficient are also higher than the carbon-based processes in the 5000 K – 15000 K range. This particular combination of properties is likely to have a very significant impact on the dynamics, stability, and electrical behaviour of the plasma arc in these cases.

MHD plasma arc simulations

The plasma properties shown in the previous section were taken forward into computational MHD simulations with the plasmaArc 1.0.0 solver to study the effect of various reductant and process routes on the stability and electrical behaviour of the arc in a hypothetical DC furnace operation. The arc was simulated in a simplified furnace geometry configured with a vertically mounted graphite electrode acting as the cathode (electrical negative), a flat bath of process material below it acting as the anode (electrical positive, connected to ground), and a hemispherical region of the furnace freeboard gas space around the electrode tip. The unstructured polyhedral computational mesh was anisotropically refined in the volume between the electrode tip and the anode where the arc is usually located. This geometry is illustrated visually in Figure 10.

Parameters used in the MHD models are shown in Table 2, and were set to these values in all cases unless otherwise indicated. The new CASM-style temperature boundary conditions were implemented on the anode and cathode surface with parameters as shown in Table 3, where properties were selected based on the boundary materials (graphite for the cathode, and molten slag for the anode).

Numerical tests – mesh dependence behaviour

Numerical testing of the MHD model was performed in two steps. The first of these involved varying the spatial resolution of the elements in the computational mesh, represented by Δ_m. For these tests, the "50 kA scale" case parameters in Table 2 were used together with the plasma properties calculated for the ConRoast® process using coke reductant and a slag bath temperature of 2500°C. Instantaneous maximum values of the temperature and velocity fields were extracted from the simulation results as a function of time, along with total voltage drop across the arc (calculated as the difference between minimum and maximum values of the electric potential field). Average and standard deviation values were then calculated from this data and reported as a function of Δ_m. The results are shown in Figure 11.

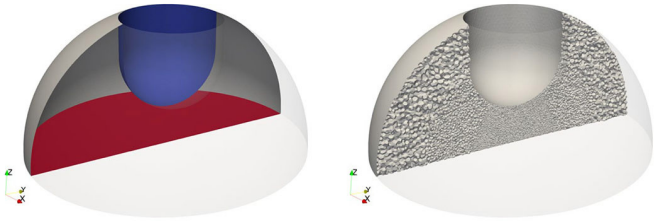

Figure 10—(l) geometry of MHD model domain, (r) computational mesh used for numerical solution

Although it is clear that the MHD model is not fully mesh-independent at the range of resolutions tested, the sensitivity of the results to mesh resolution is relatively low. This is particularly true for the calculated arc voltage, which is an important parameter in the electrical design of transformers and rectifiers for DC furnace power supplies. At mesh resolutions $\Delta_m < 10$ mm the average and standard deviations of the arc voltage do not change significantly, and 7.5 mm was chosen as a suitable value for the remainder of this study.

Table 2

Model parameters used in MHD simulations

Parameter	5 kA scale	50 kA scale
Current, I	5 kA	50 kA
Arc length, L_a	0.2 m	0.2 m
Electrode diameter, D_e	0.2 m	0.5 m
Region diameter, D_r	0.8 m	1.4 m
Ambient freeboard temperature, T_{fb}	1923 K	1923 K
Cathode spot current density, $\|\mathbf{j_B}\|$	2 x 10^7 A/m^2	1 x 107 A/m^2
Mesh resolution (arc region), Δ_m	7.5 mm	7.5 mm
Total run time, t_s	50 ms	50 ms

Table 3

Parameters for CASM temperature boundary conditions

Parameter	Cathode boundary	Anode boundary
Work function, W_f	4.62 V	4 V
Richardson-Dushman constant, A_{RD}	6 x 10^5 A/m^{2}K^2	6 x 105 A/m^{2}K^2
Vaporisation temperature, T_v	4100 K	3500 K
Bulk electrode temperature, T_∞	1923 K	1923 K
Boundary density, ρ_B	1500 kg/m^3	3500 kg/m^3
Boundary heat capacity, $C_{P,B}$	1000 J/kg.K	1000 J/kg.K
Boundary heat transfer coefficient, h_B	2500 W/m^{2}K	2500 W/m^{2}K
Active layer thickness, δ_B	10^{-5} m	10^{-5} m

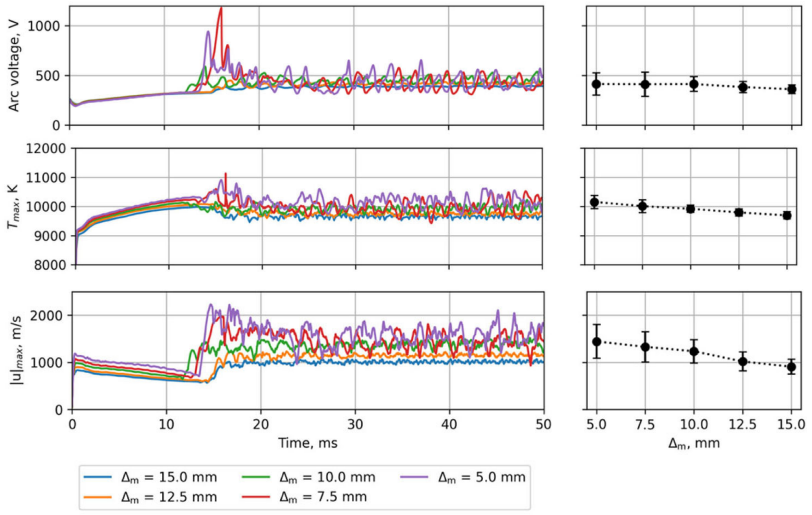

Figure 11—Mesh dependence behaviour in MHD model: ConRoast® with coke reductant, T_s = 2500°C, 50 kA scale (error bars show one standard deviation)

Numerical tests – model validation

The second test of numerical performance involved comparing the model's predictions of the voltage-current-arc-length relationship to those reported in literature. Empirical expressions for the shape of the arc column, and hence, the voltage as a function of arc length and current, have been developed for DC arcs by Bowman (Bowman, Krüger, 2009). Bowman's formula conveniently characterises the arc's electrical characteristics using a single parameter, that is, the arc resistivity. Based on extensive measurements from pilot-scale PGM alloy smelting tests Jones (2015) established a representative value of 0.0175 Wcm for the arc resistivity in such processes, with a likely range between 0.015 Wcm and 0.020 Wcm. These empirical calculations were compared to results from the MHD model at 50 kA scale, again using the ConRoast® and coke case. The arc length L_a (defined here as the distance between the tip of the electrode and the molten bath) was varied between 5 cm and 30 cm. Two sets of simulation results were obtained, one using plasma properties associated with a slag temperature of 1650°C, and one at 2500°C. The arc voltage behaviour is shown in Figure 12.

It is interesting to observe that, while the MHD model generally over-predicts the arc voltage compared to the Bowman equation, the results when using plasma properties associated with a slag temperature of 2500°C are more realistic and stay mostly within one standard deviation of the Bowman results. This suggests that evaporation of process material from the superheated arc attachment zone and its subsequent interaction with the arc may be a significant effect in real furnaces.

Process comparisons

Once testing was completed, the MHD model was applied to the problem of reductant choice in PGM alloy smelting and its impact on the electrical behaviour of the plasma arc in such processes. In order to do this, a comprehensive test matrix was developed covering four parameters: raw material (either autocats or ConRoast® oxidised concentrate), slag temperature used for gas-phase composition calculations (1650°C or 2500°C), current scale (5 kA or 50 kA), and reductant material (metallurgical coke, SiC, FeSi, or H_2). Accounting for all possible combinations results in 32 different simulation cases. For each case, all other model parameters were fixed at the values shown in Table 2 and Table 3. The arc

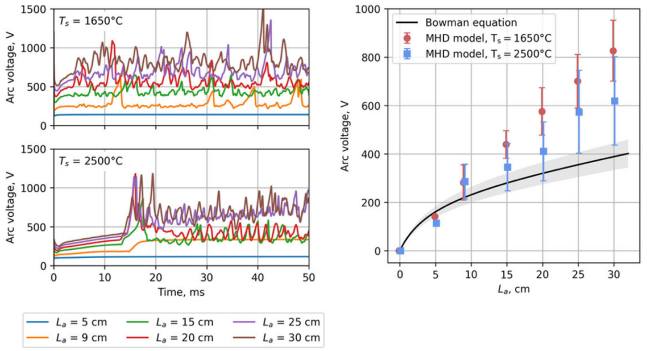

Figure 12—Comparison between MHD model and Bowman empirical calculation: ConRoast® with coke reductant, 50 kA scale (error bars show one standard deviation)

voltage data from each simulation was analysed as before to obtain averages and standard deviations.

Starting with processes using ConRoast® raw material, a summary of the arc voltage results from the simulation cases is shown in Figure 13. Several broad trends may be observed: Firstly, processes using Coke, SiC, and FeSi reductants all produce roughly the same voltages at equivalent currents. Arcs in a hydrogen-reduction atmosphere exhibit somewhat higher voltages, especially at T_s = 1650 °C, where the furnace atmosphere is close to being a pure mixture of H_2 and Ar. Secondly, the slag temperature affects the arc behaviour significantly via its effect on the freeboard gas composition, and hence, the plasma properties. This is because higher slag temperatures produce a freeboard gas with more metallic contaminants, and hence, much higher electrical conductivity and radiation emission coefficients at typical arc plasma temperatures. Interestingly, the effect on the MHD model is reversed depending on scale – at 50 kA, the higher conductivity at lower temperatures means the conducting volume of the arc is increased, and the large diameter of the arc column means that most of the increased radiation emission is recaptured. This results in a more conductive arc, and a decrease in the arc voltage. At 5 kA scale, the higher radiation emission from the body of the arc causes the plasma to cool rapidly as it passes along the length of the arc jet, and this cooling effect dominates over any increase in plasma conductivity – this results in a more resistive arc, and a corresponding increase in the arc voltage.

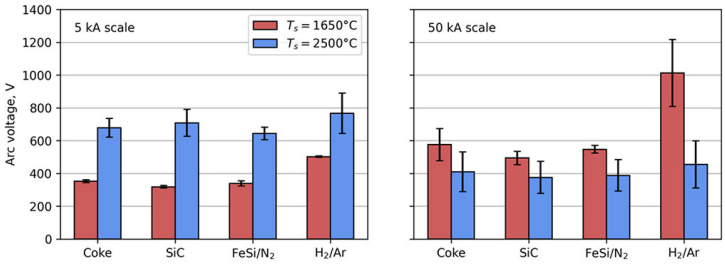

Figure 13—MHD model arc voltages for process combinations using ConRoast® raw material (*l*) 5 kA scale, (*r*) 50 kA scale (error bars show one standard deviation)

A set of visualisations of the plasma temperature field from the ConRoast® simulation cases is shown in Figure 14 and Figure 15. These visualisations present the instantaneous state of the field at the end of the simulation, that is, 50 ms. The colours represent a temperature range of 1923 K (blue) to 6000 K (red), with the three-dimensional 6000 K isotherm in grey to give an indication of the shape of the arc column. At 5 kA scale it can be seen that the arc is generally close to steady-state and axisymmetric when operating in gas generated by slag at 1650°C (although the size and shape of the arc is affected by the choice of reductant), but the size of the column shrinks dramatically due to excessive radiative cooling when operating in gas from slag at 2500°C. This also triggers some dynamic behaviour, with helical flow instabilities twisting the arc into an oscillating spiral shape. At 50 kA scale the arcs are all highly dynamic in their behaviour with a combination of turbulent and electromagnetic instabilities, and although the arc columns are more compact when operating in gas generated by slag at 2500°C, the change is not as extreme as in the 5 kA case.

Moving on to the autocat recycling process, the arc voltage results obtained from this set of cases are given in Figure 16. Comparison with Figure 13 shows that there is a remarkable degree of similarity in both the absolute values and broader trends in the modelled voltages. This is perhaps unsurprising, given that the calculated plasma properties for a given combination of reductant and slag temperature were earlier seen to be very similar, regardless of the raw material being smelted.

Visualisations of the temperature field for the autocat process cases are shown in Figure 17 and Figure 18. Again, there is considerable similarity with the results obtained from the ConRoast® cases, with the arc's dynamics and spatial structure following the same trends.

Conclusions

A computational modelling workflow to study the effect of metallurgical process changes on plasma arc behaviour was successfully developed for the case of PGM alloy smelting. This workflow was used to examine the impact of the use of alternative reductants in the ConRoast® and autocat smelting processes in order to reduce their carbon emissions.

In the first step of the workflow, the freeboard gas compositions were calculated using thermochemical models. This showed that gas

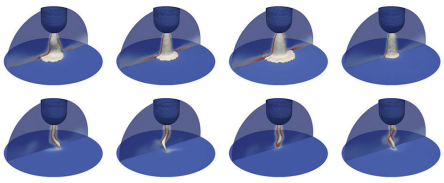

Figure 14—Visualisations of the plasma temperature field from ConRoast® simulation cases at 5 kA (*l* to *r*): Coke, SiC, FeSi, and H_2 reductants, (*t* to *b*): 1650°C and 2500°C slag temperatures

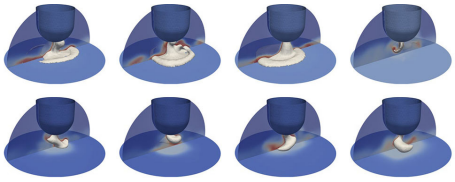

Figure 15—Visualisations of the plasma temperature field from ConRoast® simulation cases at 50 kA (*l* to *r*): Coke, SiC, FeSi, and H_2 reductants, (*t* to *b*): 1650°C and 2500°C slag temperatures

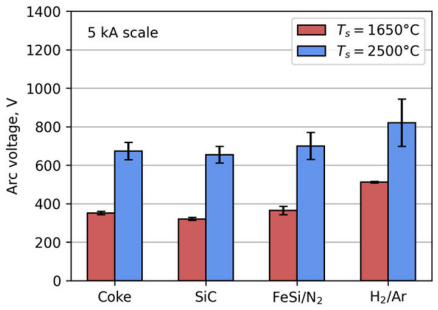

Figure 16—MHD model arc voltages for process combinations using autocat raw material (*l*) 5 kA scale, (*r*) 50 kA scale (error bars show one standard deviation)

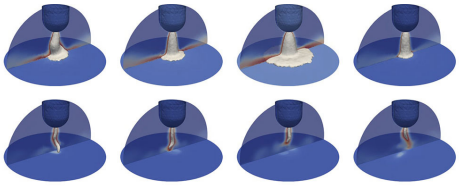

Figure 17—Visualisations of the plasma temperature field from autocat simulation cases at 5 kA (*l* to *r*): Coke, SiC, FeSi, and H_2 reductants, (*t* to *b*): 1650°C and 250 0°C slag temperatures

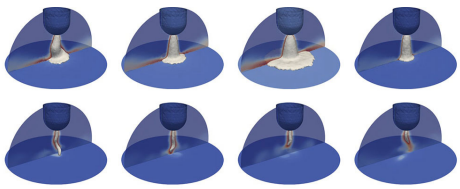

Figure 18—Visualisations of the plasma temperature field from autocat simulation cases at 50 kA (*l* to *r*): Coke, SiC, FeSi, and H_2 reductants, (*t* to *b*): 1650°C and 2500°C slag temperatures

compositions associated with metallurgical coke and SiC reductants were predominantly carbon monoxide, while freeboard gas from FeSi reductants contained mostly nitrogen from the purge gas, and the use of hydrogen reductant resulted in a gas containing mostly hydrogen with small amounts of water vapour. When the slag temperature was increased as might be expected in the superheated arc attachment zone in a DC smelting furnace, the gases became increasingly contaminated with other elements such as metals, silicon, and sulphur. The gas-phase composition of minor elements

associated with autocat smelting was seen to be less complex than that from the ConRoast® process, owing to the relative purity of the different raw materials used.

The calculated gas compositions were taken into equilibrium plasma calculations to compute the thermophysical properties of plasmas obtained from heating the freeboard gas compositions to high temperatures. A high degree of similarity in the plasma properties was observed between autocat and ConRoast® processes when using the same reductant and slag temperature. The plasma properties were also broadly similar between metallurgical coke, SiC, and FeSi reductants, with more significant differences observed in the plasma density and heat capacity when H_2 reductant was used. Large differences were seen when the slag temperature (and associated equilibrium gas composition) was changed from 1650°C to 2500°C, with higher slag temperatures producing plasmas with higher electrical conductivity and thermal radiation emission coefficients.

The plasma property data sets were then used in computational MHD models to simulate arc behaviour under different conditions of raw material, reductant choice, slag temperature, and furnace scale. In general, the arc voltages obtained from the simulations were similar between coke, SiC, and FeSi reductants, while using H_2 resulted in more resistive arcs with higher voltages. At 5 kA current scale the arc voltages increased significantly when the slag temperature was increased from 1650°C to 2500°C due to excessive radiative cooling of the arc column, whereas at 50 kA scale this trend was reversed with arc voltages dropping as slag temperature increased due to increased plasma electrical conductivity. Between ConRoast® and autocat smelting, quantitative and qualitative differences in arc behaviour were seen to be negligible when the remaining parameters of current scale, reductant, and slag temperature were the same.

This work remains exploratory and theoretical in nature at present, and can certainly be improved on by future research in several ways. First and foremost, experimental testing of these processes at laboratory or pilot plant scale would provide invaluable data for better validation of the modelling results. Direct measurement of gas compositions in the general freeboard space and in the central arc region, although challenging, would also be of great use in refining the input data for the models. Improvements to the computationally expensive MHD modelling step would also be of great use, both in the area of refining existing models with improved and more accurate physics, and to develop new generations of reduced-order models, which require fewer computational resources.

Acknowledgements

This paper is published with the permission of Mintek, and was supported by funding from Mintek Science Vote project IntelliMetTwin MCR-62604. The authors acknowledge the Centre for High Performance Computing (CHPC) South Africa, for providing computational resources to this research project.

References

Akhmetov, A., Zulhan, Z., Sadyk, Z., Burumbayev, A., Zhakan, A., Kabylkanov, S., Toleukadyr, R., Saulebek, Z., Ayaganova, Z., Makhambetov, Y. 2025. Carbon-Free Smelting of Ferrochrome Using FeAlSiCa Alloy. *Processes,* vol. 13, p. 1745. https://doi.org/10.3390/pr13061745

Al Nasser, M., Alrasheedi, N., Karimi-Sibaki, E., Vakhrushev, A., Ahmadein, M., Ataya, S., Kharicha, A. 2024. Exploring Extreme Voltage Events in Hydrogen Arcs within Electric Arc Furnaces. *Sustainability,* vol. 16, p. 2831. https://doi.org/10.3390/su16072831

Bale, C.W., Bélisle, E., Chartrand, P., Decterov, S.A., Eriksson, G., Gheribi, A.E., Hack, K., Jung, I.-H., Kang, Y.-B., Melançon, J., Pelton, A.D., Petersen, S., Robelin, C., Sangster, J., Spencer, P., Van Ende, M.-A. 2016. FactSage thermochemical software and databases, 2010–2016. *Calphad*, vol. 54, pp. 35–53. https://doi.org/10.1016/j.calphad.2016.05.002

Barcza, N.A., Curr, T.R., Jones, R.T. 1990. Metallurgy of open-bath plasma processes. *Pure and Applied Chemistry*, vol. 62, pp. 1761–1772. https://doi.org/10.1351/pac199062091761

Benson, M., Bennett, C.R., Harry, J.E., Patel, M.K., Cross, M. 2000. The recovery mechanism of platinum group metals from catalytic converters in spent automotive exhaust systems. *Resources, Conservation and Recycling Journal*, vol. 31, pp. 1–7. https://doi.org/10.1016/S0921-3449(00)00062-8

Bowman, B., Krüger, K. 2009. Arc Furnace Physics. Verlag Stahleisen GmbH, Düsseldorf, Germany.

Dalaker, H., Hovig, E.W. 2023. *Hydrogen Plasma-Based Reduction of Metal Oxides*, in: Fleuriault, C., Steenkamp, J.D., Gregurek, D., White, J.F., Reynolds, Q.G., Mackey, P.J., Hockaday, S.A.C. (Eds.), Advances in Pyrometallurgy, The Minerals, Metals & Materials Series. Springer Nature Switzerland, Cham, pp. 85–94. https://doi.org/10.1007/978-3-031-22634-2_8

Geldenhuys, I.J. 2017. The Exact Art and Subtle Science of DC Smelting: Practical Perspectives on the Hot Zone. *The Journal of the Minerals,* vol. 69, pp. 343–350. https://doi.org/10.1007/s11837-016-2171-z

Jones, R.T. 2015. Fundamental aspects of alloy smelting in a DC arc furnace (Ph. D.). University of the Witwatersrand, Johannesburg.

Jones, R.T. 2002. ConRoast: DC arc smelting of dead-roasted sulphide concentrates, in: Sulfide Smelting '02. Presented at the *Third International Sulfide Smelting Symposium*, TMS Annual Meeting, Seattle, Washington, USA, p. 22.

Lowke, J.J., Morrow, R., Haidar, J. 1997. A simplified unified theory of arcs and their electrodes. *Journal of Physics*, vol. 30, pp. 2033–2042. https://doi.org/10.1088/0022-3727/30/14/011

Malan, W., Akdogan, G., Bradshaw, S., Bezuidenhout, G. 2015. The recovery of platinum group metals from low-grade concentrates to an iron alloy using silicon carbide as reductant. *The Journal of the Southern African Institute of Mining and Metallurgy*, vol. 115, no. 5, pp. 375–383. https://doi.org/10.17159/2411-9717/2015/v115n5a5

Morcali, M.H. 2020. A new approach to recover platinum-group metals from spent catalytic converters via iron matte. *Resources, Conservation and Recycling Journal,* vol. 159, 104891. https://doi.org/10.1016/j.resconrec.2020.104891

OpenCFD Ltd. 2025. *OpenFOAM v2506*, https://www.openfoam.com/ [WWW Document]. https://www.openfoam.com/ (accessed 8.17.25).

Peng, Z., Li, Z., Lin, X., Tang, H., Ye, L., Ma, Y., Rao, M., Zhang, Y., Li, G., Jiang, T. 2017. Pyrometallurgical Recovery of Platinum Group Metals from Spent Catalysts. *The Journal of the Metals,* vol. 69, pp. 1553–1562. https://doi.org/10.1007/s11837-017-2450-3

Phillips, R.E., Jones, R.T., Chennells, P. 2008. Braemore Platinum Smelters: Commercialization of the ConRoast process, in: Platinum in Transformation. Presented at the *Third International Platinum Conference*, The Southern African Institute of Mining and Metallurgy.

Reynolds, Q.G. 2025. *plasmaArc*, https://github.com/quinnreynolds/plasmaArc/releases/tag/v1.0.0-openfoam-v2412

Reynolds, Q.G. 2020. Toward computational models of arc dynamics in silicon smelters. 14th International Conference on CFD in the Oil & Gas, Metallurgical and Process Industries. Presented at the *14th International Conference on CFD in the Oil & Gas, Metallurgical and Process Industries*, SINTEF Academic Press, Trondheim, Norway, pp. 99–106.

Reynolds, Q.G., Bowman, B., Erwee, M.W., Geldenhuys, I.J., Sandrock, C., Venter, G.A., Xakalashe, B.S., Zietsman, J. 2025a. Plasma soup for the pyrometallurgist's soul. *The Journal of the Southern African Institute of Mining and Metallurgy*. vol. 125, pp. 129–144. https://doi.org/10.17159/2411-9717/758/2025

Reynolds, Q.G., Sandrock, C., Goutier, P.-A. 2025b. *minplascalc*, https://github.com/quinnreynolds/minplascalc/releases/tag/v1.0.2

Sævarsdóttir, G.A., Pálsson, H., Jónsson, M.T., Bakken, J.A. 2006. Electrode Erosion due to High-Current Electric Arcs in Silicon and Ferrosilicon Furnaces. *Steel Research International*. vol. 77, pp. 385–391. https://doi.org/10.1002/srin.200606403 ◆